Supporting Online Material for

Metasomatized Lithosphere and the Origin of Alkaline Lavas

Sébastien Pilet,* Michael B. Baker, Edward M. Stolper

*To whom correspondence should be addressed. E-mail: sebastien.pilet@unil.ch

Published 16 May 2008, *Science* **320**, 916 (2008)
DOI: 10.1126/science.1156563

This PDF file includes:

Materials and Methods

Figs. S1 to S5

Tables S1 to S3

References

1. Samples and Methods

1.1. Starting Materials

The starting materials for this study were selected from various hydrous lithospheric veins from the French Pyrenees (sampling localities: Etang de Lherz, Castillon-en–Couserans, Argein, Espeche and Avezac) (*S1, S2*). The hornblendite, AG4, and clinopyroxene (*cpx*)-hornblendite, AG7, were selected base on the fact that their amphibole compositions are characteristic of those found in metasomatic veins worldwide (Fig. 2 and S2). As we discuss in the main article, we do not think that individual veins are representative of low-degree partial melts of mantle peridotite (± volatiles); i.e., vein compositions do not represent liquid compositions. Instead, the veins are the "cumulate" residues produced by fractional crystallization of low-degree mantle melts as they ascend and cool within the lithosphere. Depending on pressure and liquid volatile content, such a process may well generate a continuum from anhydrous to hydrous phase assemblages (*S3-S6*). Figure S3 shows that while the whole-rock compositions of various Pyrenean amphibole-bearing veins cover a large range, the compositions of the amphiboles within the veins are much more restricted in composition. Thus, the bulk-rock vein compositions reflect the modal abundance of amphibole relative to nominally anhydrous minerals, e.g., amphibole (*amph*) + minor Fe-Ti oxides for AG2 and 4, *cpx* + *amph* for AG7, and *cpx* + olivine (*ol*) + *amph* for AG6 and 1, rather than the bulk composition of any basanitic liquid. Another important point to stress is that the compositions of amphiboles from Pyrenean metasomatic veins are similar to the compositions of amphiboles that crystallize from *ne*-normative (*S7*) to *hy*-normative (*S8*) experimental liquids (Fig. S3). This suggests that the amphibole in our starting

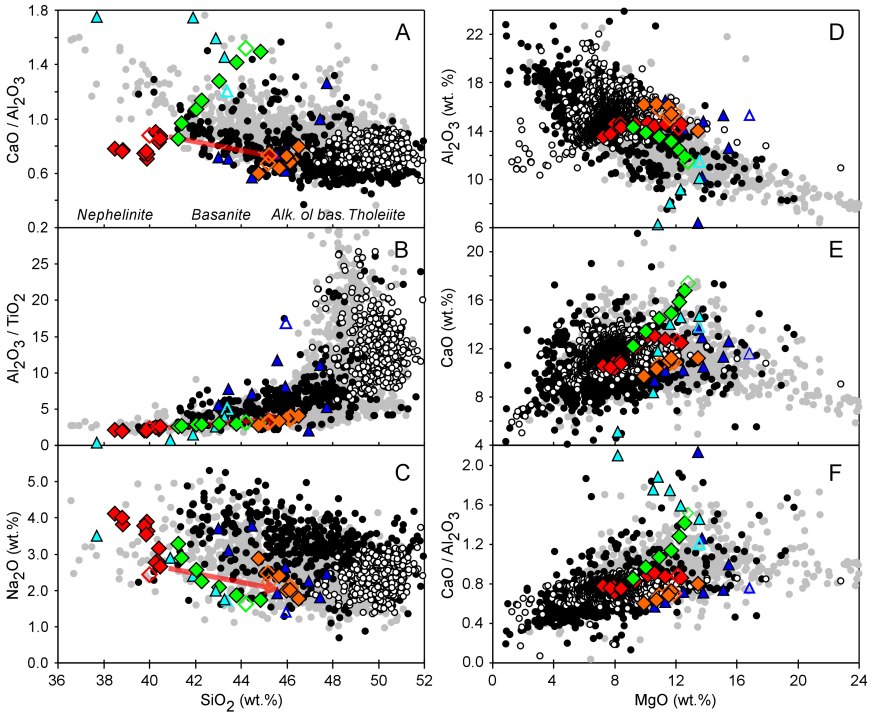

Fig. S1. Major-element oxides or oxides ratios vs. SiO_2 or MgO (volatile-free) in the partial melts of AG4 and AG7 (this study), and silica-deficient *gt* pyroxenites either with (*S39*) or without CO_2 (*S40, S41*) relative to continental and oceanic intraplate basalt and MORB compositions; (A) CaO/Al_2O_3 vs. SiO_2, (B) Al_2O_3/TiO_2 vs. SiO_2, (C) Na_2O vs. SiO_2, (D) Al_2O_3 vs. MgO, (E) CaO vs. MgO, and (F) CaO/Al2O3 vs. MgO. Filled grey circles: OIBs; filled black circles: continental intraplate basalts; filled white circles: MORBs (all rock compositions from GEOROC and PetDB databases; plotted rocks have 8-15 wt. % MgO in panel A to C and have SiO_2 wt. % below 52 in panel D to F). Filled dark blue triangles: glass compositions from 2-5 GPa experiments on silica-deficient *gt* pyroxenites (open dark blue triangle is the starting composition) (*S40, S41*). Filled light blue triangles: glass compositions from 3 GPa experiments on silica-deficient *gt* pyroxenites with 5 wt. % CO_2 (open light blue triangle is the starting composition) (*S39*). Filled red diamonds: hornblendite AG4 melts (open red diamond: starting material). Filled green diamonds: clinopyroxene hornblendite AG7 melts (open green diamond: starting material). Orange filled and open diamonds: melts from hornblendite AG4 – Depleted MORB mantle (DMM1) sandwich experiments with and without *opx* observed in peridotitic layer, respectively. Positions of the terms Nephelinite, Basanite, Alkali olivine basalt (Alk. ol bas.), and Tholeiite along the bottom of panels A denote the approximate silica values of each rock type.

material could have crystallized from a melt at moderate pressures (0.93 to 1.5 GPa), and supports the interpretation that the amphibole-bearing veins represent cumulates produced by fractional crystallization of hydrous melts as these melts move through the lithospheric mantle.

1.2. Sample description and preparation

The samples of the veins used as starting materials were cut and crushed to a size range of 1~2 mm. Unaltered material was picked under a binocular microscope and powdered using a W-carbide grinder. The powder was further ground under ethanol using a mechanical mortar and pestle until the vast majority of the grains were <10 μm in size (a few grains of augite from clinopyroxene hornblendite AG7 lay in the range 10-20 μm). The major- and minor-element compositions of both powders were determined by XRF; trace-element compositions were measured by LA-ICP-MS on fused glass pellets (both sets of measurements were made at the University of Lausanne; the LA-ICP-MS measurements are described in detail below). The CO_2 content of the starting materials, 0.20±0.05 wt% and 0.26±0.05 wt% for AG4 and AG7, respectively, was measured on 50 mg of ground rock powder by carbon-coulometry at the University of Lausanne. The water content of crushed AG4 material was measured using two different techniques. First, ~70 micrograms of vein AG4 (with a particle size of 45-60 microns) were analyzed by a micro-analytical mass spectrometric technique developed at Caltech (*S9*); the average of four measurements (n) is 1.79±0.05 (1σ). Second, a short duration piston-cylinder experiment (30 min) was performed at 1350°C and 1.5 GPa in an $Au_{75}Pd_{25}$ capsule. The H_2O content of the quenched glass (1.72±0.21 wt. % 1σ, n=5) was then analyzed by Fourier transform infrared (FTIR) spectroscopy at Caltech following the approach of Dixon *et al.* (*S10*). Details of the FTIR measurements are reported below. The average of the two mean values is 1.75±0.24 wt. %. The water content of the *cpx* hornblendite AG7 (0.76 ± 0.01 wt. % 1σ, n=4) was obtain by FTIR measurements on a 48h experiment performed at 1400°C and 1.5 GPa in a graphite-Pt capsule (AG7-12). Runs of similar duration using AG4 showed no significant water loss relative to the accepted water content of this starting material. The whole-rock compositions of AG4 and AG7 are listed in Table S1. The mode of hornblendite AG4 calculated by major-element mass balance is 96 wt.% *amph* (K-Ti-Fe pargasite), 2 wt. % Fe-Ti oxides, 1% wt. % sphene, and minor (<1 wt. %) allanite and carbonate; the mode of AG7 is 55 wt. % *amph* (K-Ti-Fe pargasite), 44 wt. % *cpx* with minor amounts of Fe-Ti oxides, carbonate, and sphene.

The peridotite material used in the hornblendite-peridotite sandwich experiments is based on the moderately depleted peridotite DMM1 described by Wasylenki *et al.* (*S11*), and was constructed using the same mineral splits and percentages. This material is composed of a mixture of natural *ol* (62.8 wt. %), orthopyroxene (*opx*) (28.4 wt. %), natural and synthetic *cpx* (8.1 wt. %), and spinel (*sp*) (0.6 wt. %). A list of the mineral compositions and a description of their preparation can be found in Wasylenki *et al.* (*S11*).

1.3. Experimental methods

For each experiment, the starting material was packed into a graphite crucible, which in turn was then placed in a 0.15 inch O.D. Pt capsule. Graphite powder was then packed on top of the graphite crucible and the open end of the Pt capsule was crimped. After drying the composite capsule for >12h at 110°C, the crimped end of the Pt capsule was welded shut.

All experiments were conduct in a 1.27 cm piston cylinder apparatus using CaF_2 cells, straight-walled graphite furnaces, and inner pieces of crushable MgO that had been dried at 1000°C for at least 12h. Pressure was applied using the hot-piston-in technique with no friction correction. $W_{97}Re_3/W_{75}Re_{25}$ thermocouples were used to monitor and control temperature to within ~1°C of the set point. The precision of the temperature measurements are thought to be ±10°C. All experiments were performed at 1.5 GPa. The experiment temperatures and run durations are reported in Table S1. N_2 gas was bled into the slot in the thermocouple plate during each experiment to minimize oxidation of the thermocouple wires within and just below the steel base plug. At the end of each experiment, the thermocouple wires just below the base plug (i.e., within the run assembly) were inspected for signs of oxidation; no evidence of significant oxidation was observed on any of the wires. The runs were quenched by turning off the electric power. For each run, the position of the capsule with respect to the center of the furnace and the position of the thermocouple tip relative to the top of the capsule were measured to ensure that the capsule was properly positioned within the furnace and that the thermocouple tip was <1 mm from the top of the capsule.

Each capsule was vertically cut using a wire-saw, and one part was mounted in epoxy for microprobe and LA-ICP-MS measurements, while the other part was doubly-polished for H_2O and CO_2 measurements using FTIR spectroscopy.

1.4. Analytical techniques

Wavelength-dispersive electron microprobe analyses of the run products were obtained at Caltech using a JEOL JXA-8200 (5 spectrometer) electron microprobe. A 15 KeV accelerating voltage was used for all analyses. Glasses were analyzed with a 10 nA broad beam (20 μm in diameter); crystalline phases were analyzed with a 20 nA focused beam (~1 μm). All data were processed using CITZAF (*S12*). USGS glasses BCR-2g, BHVO-2g and BIR-1g were analyzed during each microprobe session.

H_2O and CO_2 contents of the experimental glasses were determined using FTIR spectroscopy and the approach of Dixon *et al.* (*S10*). Transmission spectra were collected with a Nicolet Continuum Infrared Microscope connected to a Nicolet 860 Magna series FTIR using a globar source, a KBr beamsplitter, and a MCT/A detector. The experimental samples were thinned to 15-120 μm depending on the expected volatile content and were polished on both sides. The thickness for each sample was based on the average of 2-4 measurements taken on the same analyzed area after each analysis (uncertainty on the thickness is ~0.3 μm (1σ, n = 2 to 4)). The concentration of total dissolved water was calculated from the intensity of the absorption band at ~3550 cm^{-1}. The molar absorptivity of this band was taken to be 63 L/mol cm (*S13*). The CO_2 contents of the experimental glasses were determined using the doublet absorption band at ~1515 and 1435 cm^{-1}. The molar absorptivity of these bands (360 L/mol cm) was calculated for a basanite composition using the parameterization of Dixon *et al.* (*S14*).

Laser ablation inductively coupled plasma mass spectrometry (LA-ICP-MS)

analyses of the glasses were carried out at the University of Lausanne using an EXCIMER laser (193 nm) coupled to a Perkin-Elmer ELAN 6100 DRC ICP-MS (see also Günter *et al.* (*S15*)); laser settings: 10 Hz, fluency ~13 J/cm^2; acquisition time: gas blank ~ 60s, data ~ 40s. The spot size varied from 20 to 60 µm and was dictated by the size of the glass pools being analyzed. Data were reduced using the CONVERT and LAMTRACE programs (*S16*). NIST612 glass was used as an external standard and the CaO content of each glass (from the electron microprobe measurements) served as an internal standard. The trace element contents of the experimental glasses are presented in Table S3 and correspond to the average of four analyses on each glass; within the measurement uncertainty, no compositional variation is observed within the glasses in any of the experiments. BCR-2 glass was monitored during all analytical sessions and treated as an unknown during data reduction. Based on 20 BCR-2g measurements, the relative errors on the trace element contents in the unknowns lie between 5-14%.

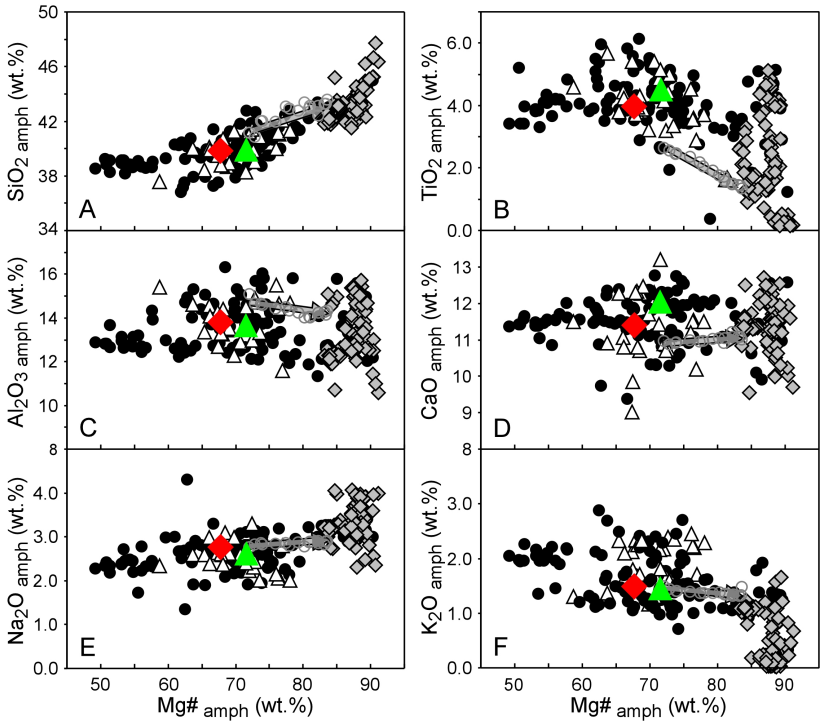

Fig S2. Mg# (100Mg/(Mg+Fe) molar) vs. selected oxide wt% values in amphiboles from the starting compositions AG4 (filled red diamond) and AG7 (filled green triangle) as well as from amphiboles in oceanic and continental lithospheric veins (filled black circles), in continental basanite xenocrysts (open black triangles), and in peridotites from xenoliths and ophiolites (grey diamonds); (A) SiO_2, (B) TiO_2, (C) Al_2O_3, (D) CaO, (E) Na_2O, and (F) K_2O. The error bars associated with amphibole from hornblendite AG4 and AG7 correspond to one standard deviation; in most cases error bars are smaller than the symbols. The open grey circles correspond to the compositional variation of amphiboles from the center (low Mg#) to the edge (high Mg#) in a lithospheric vein in contact with peridotite (*S42*); this compositional trend is also shown by the grey arrow in each panel. Note that the compositions of amphibole in lithospheric veins show a large range of Mg#s (from 50 to 90) and high TiO_2 (3.3-6 wt%) and K_2O (1-3 wt%) contents; Al_2O_3, CaO, and Na_2O contents are relatively independent of Mg#. Compared to the compositions of the vein amphiboles, amphiboles from metasomatized peridotites have systematically higher Mg#s, similar Al_2O_3, CaO, and Na_2O contents, and a wider range of TiO_2 and K_2O values. The core to rim trend of decreasing TiO_2 content with increasing amphibole Mg# (as a result of partial re-equilibration of vein amphiboles with the enclosing peridotite) (*S42*) suggests that amphiboles within a single lithospheric vein may have a range of Mg#s and TiO_2 contents and that amphibole from lithospheric veins with high Mg# (>80) could have re-equilibrate with surrounding peridotite. Note that the partial re-equilibration does not appear to affect the CaO, Al_2O_3, Na_2O, and K_2O contents. The compositions of amphibole megacrysts carried by continental basanites completely overlap the compositions of amphibole in lithospheric veins, and the amphibole in hornblendite AG4 and clinopyroxene hornblendite AG7 are representative of the range of amphibole compositions observed in lithospheric veins worldwide.

Sample locations: the compositions of amphibole from lithospheric veins plotted in this figure come from xenoliths carried by alkaline lavas from La Palma (*S43, S44*) (Canary Islands), Kerguelen Islands (*S45*), Iberia west passive margin *(S46*), Szigliget (*S42, S47, S48*) (Hungary), Eifel (*S48-S51*) (Germany), Nunivak (*S48*) (Alaska), Dish Hill (*S48*), and Grand Canyon (*S52*) (USA), Birket Ram (*S49*) (Israel), Bartoy & Vitim (*S53*) (Russia), Kiama area (*S54*) (Australia). In addition, amphibole compositions from lithospheric veins in mantle outcrops in the French Pyrenees are also plotted (Etang de Lherz (*S55, S56*), Castillon-en –Couserans, Argein, Espeche and Avezac, Pilet, unpublished data). The metasomatized peridotite amphiboles are from xenoliths found in the following alkaline massifs: Little Hungarian plain (*S57*) and Eastern Transylvanian basin (*S42*) (Hungary), Kapfenstein (*S57*) (Austria), Bartoy (*S53*) (Russia), La Palma (*S43*) (Canary Islands), Ataq (*S58*) (Yemen), Kerguelen Islands (*S45, S59*), Eifel (*S51*) (Germany), Iberia west passive margin (*S46*), mantle outcrops from Zabargad Island (*S57*) (Red Sea), Balmuccia (*S57*) and Premosello (*S57*) massifs (Western alps), Lherz (*S55, S57*) (Eastern Pyrenees), external ligurides (*S57*) (Northern Apennine). The amphibole megacryst compositions plotted in the figure are from alkaline basalt samples from: Black Rock (*S48*) and San Carlos (*S48*) (USA), Nandewar (*S48*) and Anakies (*S48*) (Australia), Kakanui (*S48*) (New Zealand), Elie Ness (*S48*) (Scotland), Eifel (*S48, S60*) (Germany), Sauclieres (*S48*) and Massif Central (*S61*) (France), Tenerife (*S48*) (Canary Islands), Moroto (*S48*) (Uganda), Pannonian Basin (*S47*) (Hungary).

1.5. Phase proportions and mass balance calculations

The phase proportions listed in Table S1

were calculated by mass balance using the least-square fitting approach described by Albarede and Provost (*S17*), and the following elements: SiO_2, TiO_2, Al_2O_3, FeO*, MnO, MgO, CaO, Na_2O, K_2O, P_2O_5, H_2O and CO_2. Since the CO_2 content of the glass reflects both the initial carbon content of the starting material and exchange with the graphite capsule, the CO_2 content of the starting material was treated as a variable along with the proportions of the glass and crystalline phases (i.e., during each mass balance calculation the sum of the oxides in the bulk was constrained to be 100, and thus as bulk CO_2 increased the remaining oxides decreased proportionately). The mass balance calculations indicate that water loss in the majority of our experiments was less than 10% relative; the exceptions are experiments AG4-7, -8, -21r and -38 which experienced relative water losses of 23, 17, 24 and 13 %, respectively.

1.6. Volatile contents of the experimental glasses

H_2O contents of glasses from the AG4 and AG7 melting experiments are 1.7-3.7 and 0.8-2.2 wt. %, respectively (Table S1). For each bulk composition, water contents are inversely correlated with melt fraction, consistent with the observed conservation of water based on mass balance. These H_2O contents are comparable to those estimated for undegassed alkaline magmas from Hawaii (0.5-1.9 wt. % H_2O) (*S18*). In contrast, although the veins used as starting materials contain igneous carbonate, the CO_2 contents of our experimental melts (0.7-1.21 wt. % CO_2 for AG4 and 0.6-1.14 wt. % CO_2 for AG7) are uncorrelated with melt fraction and reflect equilibration between the melt and graphite capsule at the fO_2 of each experiment. Nevertheless, these CO_2 contents are comparable to those estimated for undegassed alkaline magmas from Hawaii (1.4-4.9 wt. % CO_2) (*S18*), and since dissolved CO_2 likely influences phase equilibria, its presence in our experiments is realistic.

1.7. Approach to equilibrium

Run durations in our experiments varied from 24 to 64 h with longer run times used for the lower temperature experiments. The mass balance calculations described above indicate that with the exception of CO_2 (and to a much lesser extent H_2O) bulk composition was conserved in our experiments. Constant bulk composition is a necessary, albeit, insufficient condition for equilibrium. In all of our AG4 experiments, liquid, *ol*, and *cpx* compositions are homogeneous, i.e., with uncertainties comparable to those calculated for the USGS glasses. The AG7 experiments contain partially unreacted *cpx* cores. Relict *cpx* cores are ubiquitous in experiments on starting materials that contain *cpx* (*S19-S21*); however in our experiments these cores represent a relatively small fraction of the total *cpx* present in these capsules, i.e., the volume of the *cpx* overgrowth rims are large compared to the partially reacted cores and thus we expect that these cores do not have a large effect on the liquid compositions. $K_d^{min/liq}{}_{Fe*/Mg}$ values in our experiments are 0.264 -0.287 and 0.225-0.297 for *ol* and *cpx*, respectively. These values are slightly lower than that expected for basaltic liquids (0.3-0.35 and 0.3-0.36 for *ol* and *cpx* respectively (*S11*)) but are similar to the $K_d^{min/liq}{}_{Fe*/Mg}$ values measured in experiment where liquids contain more that ~ 4.5 wt. % Na_2O+K_2O (an inverse correlation exist between $K_d^{min/liq}{}_{Fe*/Mg}$ and liquid alkali content (*S11*)). In our amphibole-bearing experiments, the grains are homogeneous and the composition is independent of the location of the grain within the charge. Measured $K_d^{amph/liq}{}_{Fe*/Mg}$ in the low temperature AG4 experiments (0.297-0.341) are in the same range as that measured by Tiepolo *et al.* (*S7,S22*) (0.308

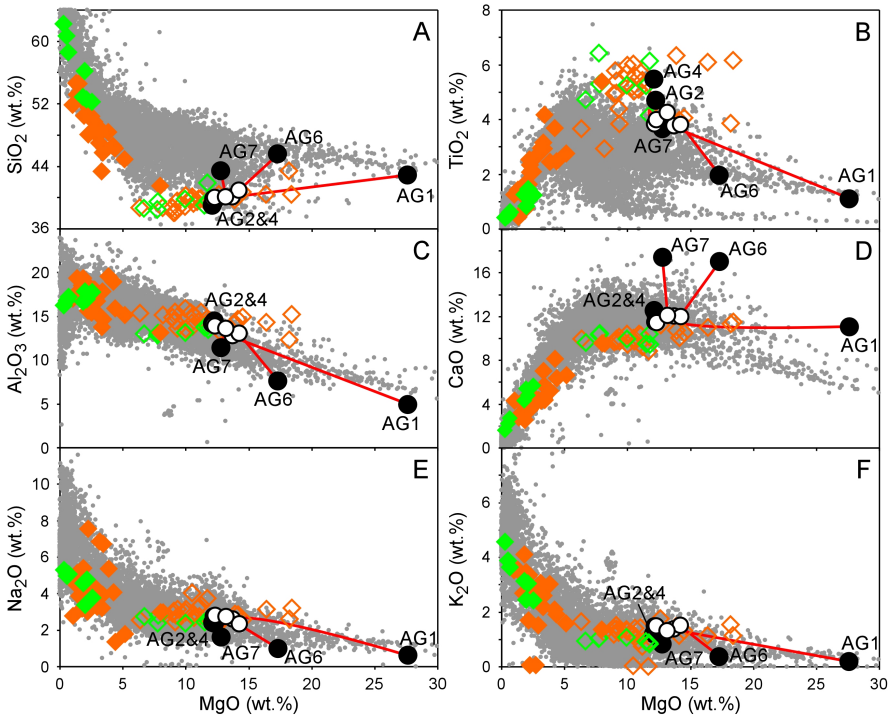

Fig. S3. Major-element oxides vs. MgO (all in wt. % on a volatile-free basis) for amphibole-bearing veins from the French Pyrenees (AG1-7) compared to OIB compositions (from the GEOROC database). In addition, the compositions of amphibole from the Pyrenean veins (AG1-7) are shown along with the compositions of experimental amphiboles (*S7*, *S8*). (A) SiO_2, (B) TiO_2, (C) Al_2O_3, (D) CaO, (E) Na_2O, (F) K_2O. Filled grey circles: OIBs (rock compositions from GEOROC database); filled black circles: whole rock compositions of amphibole-bearing veins AG1, 2, 4, 6, and 7; filled white circles: compositions of amphibole in veins AG1, 2, 4, 6, and 7. Each red line links the whole rock vein composition to its corresponding amphibole composition. The filled orange and green diamonds correspond to melt compositions in equilibrium with amphibole (open orange and green diamond) in the Tiepolo et al. (*S7*) and Nekvasil et al. (*S8*) experimental studies, respectively. This figure illustrates that the compositions of amphibole observed in lithospheric veins are independent of the whole rocks composition of the associated vein, and that the sampled whole-rock vein compositions represent various proportions of cumulate phases.

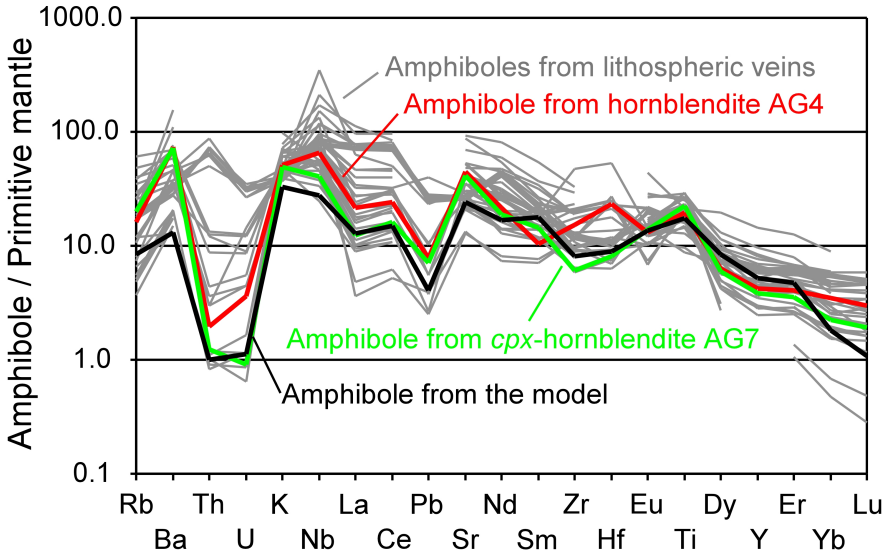

Fig. S4. Trace-element contents (normalized to primitive mantle (*S37*)) of amphibole from AG4 hornblendite and AG7 clinopyroxene hornblendite, from oceanic and continental hydrous lithospheric veins, and from the model for the formation of amphibole-bearing metasomatic veins. See text for a description of the model. Note the high trace-element contents in amphiboles from lithospheric veins and that the amphiboles in samples AG4 and AG7 (used as starting material) are representative of this global suite of samples. The wide range of Th and U contents found in this sample suite may reflect the non-uniform distribution of melt inclusions, grain boundary phases, and apatite inclusions (all are phases that are enriched in Th and U relative to the more abundant silicates in mafic and ultramafic lithologies) (*S38*). Such a non-uniform distribution of Th- and U-rich minor phases in lithospheric veins may explain the discrepancy between the bulk-rock Th and U content of hornblendite AG7 and the content of Th and U observed in nephelinite rocks worldwide (main text, Fig. 4).

Sample locations: La Palma (*S44*) (Canary Islands), Kerguelen Islands (*S45*), Eastern Transylvanian basin (*S42*) (Hungary), Eifel (*S49, S51*) (Germany), Birket Ram (*S49*) (Israel), Bartoy and Vitim (*S53*) (Russia). In addition to AG4 and AG7, other amphibole compositions from a lithospheric vein from a French Pyrenean mantle outcrop are also plotted (Etang de Lherz (*S55*), Castillon-en-Couserans, Argein, Espeche and Avezac, Pilet, unpublished data).

± 0.042, 1σ, n=19) in experiments designed to determine trace-element $K_d^{amph/liq}$ values. The homogeneity of liquid and mineral compositions and the fact that calculated $K_d^{min/liq}{}_{Fe*/Mg}$ values are similar to those from other experimental studies suggest that our experiments closely approached equilibrium.

Finally, we conducted two temperature-change experiments (*S11, S23*) to test whether liquid compositions in our experiments can change in response to changes in experimental conditions, i.e., with an increase in temperature does the liquid evolve to a composition similar to that produced in an isothermal run at the higher temperature. In these experiments, charges were initially held at 1150°C (25 h) or 1225°C (48 h) and then the temperature was increased by 25°C and the runs were continued for an additional 54 or 48 h, respectively. The glass composition of experiment AG4-21r (1200ºC-1225ºC) overlaps with that produced in the 1225°C isothermal runs (AG4-7 and -38), although in this temperature range glass composition is not a strong function of temperature. For experiment AG4-22r (1150ºC-1175ºC), the liquid composition differs from that found in AG4-11, the constant temperature run at 1175°C, however the differences are such as to suggest that the actual run temperature of AG4-22r was ~1185°C, ~10°C higher than that of AG4-11. The glass composition of AG4-22r plots on the liquid compositional trends of the isothermal experiments but at a temperature of ~1185°C. This inferred temperature difference is also consistent with the modes of the two runs: AG4-22r contains a greater melt fraction and a smaller amphibole mode than AG4-11. Thus within the limits of our temperature reproducibility (±10°C), AG4-22r represents a successful temperature change experiment and supports our claim that our experiments represent close approaches to equilibrium.

2. Trace-element constraints on the formation of metasomatic amphibole-bearing veins

A key conclusion of the main article is that major- *and* trace-element characteristics of alkaline OIBs can be explained by high degrees of melting of small volumes of trace-element-rich material (primarily amphibole-bearing veins or their dehydrated equivalents) present in the lithospheric mantle. The incompatible trace-element content and primitive mantle-normalized pattern of any liquid produced at high degrees of partial melting (≥ ~40%) reflect, primarily, the composition of the source material. Thus, the origin of amphibole-bearing lithospheric veins is an important component of our model for the origin of alkaline OIBs. Here we briefly present the initial results of a forward calculation we have done to model the trace-element contents of amphiboles in metasomatic veins starting with a low-degree partial melt of a garnet lherzolite. The purpose of the calculation is to support the widely held view (*S3, S4, S24*) that metasomatic veins are cumulates and not liquid compositions, by reproducing via fractional crystallization the trace-element patterns observed in amphiboles in these metasomatic veins. Details of the calculation will be published elsewhere.

While the compositions of silicate melts that produce metasomatic veins in the lithosphere are poorly constrained, they are generally thought to be low-degree partial melts of volatile-bearing mantle peridotite and/or supercritical fluids. Migration, cooling, and fractional crystallization of these metasomatic agents within the lithospheric mantle would generate a continuum of phase assemblages: from anhydrous (pyroxene + garnet ± olivine) to hydrous (pyroxene + amphibole ± phlogopite) that are enriched in highly incompatible elements (*S4, S24*). The fact that the major-element compositions of amphiboles in lithospheric veins worldwide are similar to amphiboles that crystallize from *ne*- to *hy*-normative liquids at pressures of 0.93 to 1.5 GPa (*S7,*

S8) (Fig. S2 and S3) supports our assertion, and one made by many other authors (*S3, S4, S24*), that these vein amphiboles are the fractional crystallization products of hydrous mantle melts.

While it is difficult to use the major-element composition of the vein amphibole to constrain the composition of the parental liquid (due to the complicated and poorly understood nature of activity-composition relations of amphibole-melt equilibria), trace-element amphibole-liquid partition coefficients are sufficiently well known to calculate a forward model in an attempt to match the trace-element contents in the amphiboles in the metasomatic veins. In general, the overall elevation of a mantle-normalized amphibole trace-element pattern will reflect the trace element abundance in the coexisting melt. However, the shape of the pattern, e.g., the positive Nb/La and Ce/Pb ratios observed in metasomatic vein amphiboles (Fig. S4) largely reflects the specific trace-element amphibole-melt partition coefficients. In the model below, we show that with respect to trace-element abundances, the metasomatic veins can be produced by fractional crystallization of low-degree hydrous mantle melts, i.e., the veins are cumulates and do not represent bulk liquid compositions.

The model is based on that of Halliday *et al.* (*S25*) and Niu and O'Hara (*S26*) for metasomatism at the periphery of a mid-ocean ridge (Fig. S5). The starting point is that some liquids produced at low degrees of partial melting at high pressures below a mid-ocean ridge are not focused to the ridge axis, but instead metasomatize the cooling oceanic lithospheric mantle off-axis. Starting with a reasonable estimate of the trace-element content of the MORB mantle (E-DMM from *S27*), we calculated the trace-element concentrations in a liquid produced near the solidus (F=1%) in the garnet-lherzolite field by accumulated non-modal fractional melting. The primitive-mantle-normalized trace-element pattern of this liquid is very different from that observed in metasomatic veins and in the amphiboles that comprise these veins (varying the degree of melting by factors of 2 to 3 does not alter this conclusion). In particular, the calculated melts do not have the observed positive Nb vs. La or negative Pb vs. Ce anomalies.

Once the near-solidus melt migrates into the lithosphere it should begin to crystallize. We have estimated a differentiation trend based on the observed mineralogical assemblages in lithospheric veins (*S3, S4, S24, S28*), experimental data (*S7, S8, S29-S33*), and thermodynamic modeling (*S34-S36*); the fractionating assemblages involve clinopyroxene, garnet, and finally amphibole. The significant point concerning these calculations is that the mantle-normalized trace-element patterns of the evolving liquids and the clinopyroxene and garnet cumulates do not even begin to match those of the metasomatic veins or their constituent amphiboles. In contrast, the model amphibole pattern overlaps the field of amphibole compositions observed in lithospheric veins worldwide (Fig. S4). In particular, the model reproduces the positive Nb vs. La and the negative Pb vs. Ce ratios as well as the slope of the REEs observed in amphiboles from these veins. While the model has a large number of free variables, it nevertheless shows that using reasonable trace-element distribution coefficients and melting and crystallization modes, it is possible to reproduce the trace-element patterns found in amphiboles in metasomatic veins via a process of fractional crystallization within the lithosphere of near-solidus peridotite melts; this in turn supports the widely held view that these veins represent cumulates.

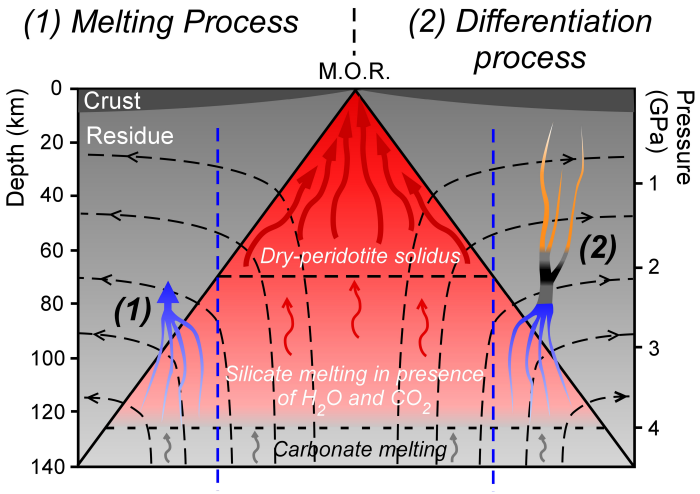

Fig. S5. Schematic model for the formation of metasomatic veins at the periphery of a mid ocean ridge (*S25, S26*). The main idea is that some liquids produced at low degrees of partial melting at high pressures below a mid-ocean ridge are not focused to the ridge axis, but instead metasomatize the cooling oceanic lithospheric mantle off-axis. This model can be separated into two phases: (1) generation of the metasomatic melt by partial melting of peridotite in the presence of H_2O and CO_2; (2) differentiation of the metasomatic melts as they move through the lithosphere and form cumulates. M.O.R.: mid-ocean ridge.

Supporting online references

S1. B. Azambre, M. Rossy, F. Albarede, *Eur. J. Mineral.* **4**, 813-834 (1992).

S2. P. Henry, B. Azambre, R. Montigny, M. Rossy, R. K. Stevenson, *Tectonophysics* **296**, 103-123 (1998).

S3. J. L. Bodinier, J. Fabries, J. P. Lorand, J. Dostal, C. Dupuy, *Bull. Mineral.* **110**, 345-358 (1987).

S4. B. Harte, R. H. Hunter, P. D. Kinny, *Philos. Trans. R. Soc. Lond. Ser. A* **342**, 1-21 (1993).

S5. J. E. Nielson, J. S. Noller, in *Mantle Metasomatism and Alkaline Magmatism* E. M. Morris, J. D. Pasteris, Eds. (Geol. Soc. Amer. Spec. Paper, 1987), vol. 215, pp. 61-76.

S6. H. G. Wilshire, in *Mantle Metasomatism and Alkaline Magmatism* E. M. Morris, J. D. Pasteris, Eds. (Geol. Soc. Amer. Spec. Paper, 1987), vol. 215, pp. 47-60.

S7. M. Tiepolo *et al.*, *Earth Planet. Sci. Lett.* **176**, 185-201 (2000).

S8. H. Nekvasil *et al.*, *J. Petrol.* **45**, 693-721 (2004).

S9. J. A. O'Leary, G. R. Rossman, J. M. Eiler, *Amer. Mineral.* **92**, 1990-1997 (2007).

S10. J. E. Dixon, E. M. Stolper, J. R. Holloway, *J. Petrol.* **36**, 1607-1631 (1995).

S11. L. E. Wasylenki, M. B. Baker, A. J. R. Kent, E. M. Stolper, *J. Petrol.* **44**, 1163-1191 (2003).

S12. J. T. Armstrong, in *Microbeam Analysis* D. E. Newbury, Ed. (San Francisco Press, San Francisco, CA, 1988) pp. 239-246.
S13. S. Newman, E. M. Stolper, R. Stern, *Geochem. Geophys. Geosyst.* 1, doi:10.1029/1999GC000027 (2000).
S14. J. E. Dixon, V. Pan, *Amer. Mineral.* **80**, 1339-1342 (1995).
S15. D. Günther, R. Frischknecht, C. A. Heinrich, H. J. Kahlert, *J. Anal. Atom. Spectro.* **12**, 939-944 (1997).
S16. H. P. Longerich, S. E. Jackson, D. Gunther, *J. Anal. Atom. Spectrom.* **11**, 899-904 (1996).
S17. F. Albarede, A. Provost, *Computers and Geosciences* **3**, 309-326 (1977).
S18. J. E. Dixon, D. A. Clague, P. Wallace, R. Poreda, *J. Petrol.* **38**, 911-939 (1997).
S19. J. M. Pickering-Witter, A. D. Johnston, *Contrib. Mineral. Petrol.* **140**, 190-211 (2000).
S20. M. B. Baker, E. M. Stolper, *Geochim. Cosmochim.* **58**, 2811-2827 (1994).
S21. D. J. Cherniak, *Chem. Geol.* **177**, 381-397 (2001).
S22. M. Tiepolo *et al.*, *Geochem. Geophys. Geosyst.* **1,** doi:10.1029/2000GC000064 (2000).
S23. X. Liu, H. St. C. O'Neill, *J. Petrol.* **45**, 1339-1368 (2003).
S24. E. M. Morris, J. D. Pasteris, *Mantle Metasomatism and Alkaline Magmatism* (Geol. Soc. Amer. Spec. Paper, Boulder, 1987), vol. 215.
S25. A. N. Halliday *et al.*, *Earth Planet. Sci. Lett.* **133**, 379-395 (1995).
S26. Y. L. Niu, M. J. O'Hara, *J. Geophys. Res.* **108**, 2209 (2003).
S27. R. K. Workman, S. R. Hart, *Earth Planet. Sci. Lett.* **231**, 53-72 (2005).
S28. F. E. Lloyd, D. K. Bailey, *Phys. Chem. Earth* **9**, 389-416 (1975).
S29. P. J. Hack, R. L. Nielsen, A. D. Johnston, **117**, 89-105 (1994).
S30. E. H. Hauri, T. P. Wagner, T. L. Grove, *Chem. Geol.* **117**, 149-166 (1994).
S31. S. Pilet *et al.*, *EOS Trans. AGU* **86**, Fall Meet. Suppl., Abstract V41E-1507 (2005).
S32. O. Muntener, P. B. Kelemen, T. L. Grove, *Contrib. Mineral. Petrol.* **141**, 643-658 (2001).
S33. O. Muntener, P. Ulmer, *Geophys. Res. Lett.* **33** (2006).
S34. M. S. Ghiorso, M. M. Hirschmann, P. W. Reiners, V. C. Kress, *Geochem. Geophys. Geosyst.* **3**, doi:10.1029/2001GC000217 (2002).
S35. M. S. Ghiorso, R. O. Sack, *Contrib. Mineral. Petrol.* **119**, 197-212 (1995).
S36. P. M. Smith, P. D. Asimow, *Geochem. Geophys. Geosyst.* **6**, doi:10.1029/2004GC000816 (2005).
S37. W. F. McDonough, S. S. Sun, *Chem. Geol.* **120**, 223-253 (1995).
S38. R. M. Bedini, J. L. Bodinier, *Geochim. Cosmochim. Acta* **63**, 3883-3900 (1999).
S39. R. Dasgupta, M. M. Hirschmann, K. Stalker, *J. Petrol.* **47**, 647-671 (2006).
S40. M. M. Hirschmann, T. Kogiso, M. B. Baker, E. M. Stolper, *Geology* **31**, 481-484 (2003).
S41. T. Kogiso, M. M. Hirschmann, D. J. Frost, *Earth Planet. Sci. Lett.* **216**, 603-617 (2003).
S42. O. Vaselli *et al.*, *J. Petrol.* **36**, 23-53 (1995).
S43. E. Wulff-Pedersen, E.-R. Neumann, B. B. Jensen, *Contrib. Mineral. Petrol.* **125**, 113–139 (1996).
S44. E. Wulff-Pedersen, E. R. Neumann, R. Vannucci, P. Bottazzi, L. Ottolini, *Contrib. Mineral. Petrol.* **137**, 59-82 (1999).
S45. B. N. Moine, M. Gregoire, S. Y. O'Reilly, S. M. F. Sheppard, J. Y. Cottin, *J. Petrol.* **42**, 2145-2167 (2001).
S46. G. Chazot, S. Charpentier, J. Kornprobst, R. Vannucci, B. Luais, *J. Petrol.* **46**, 2527-2568 (2005).
S47. G. Dobosi, H. Downes, A. Embey-Isztin, G. A. Jenner, *Neues Jahrb. Mineral.-Abh.* **178**, 217-237 (2003).
S48. J. B. Dawson, J. V. Smith, *Mineral. Mag.* **45**, 35-46 (1982).
S49. H. Downes, A. Beard, R. Hinton, *Lithos* **75**, 1-17 (2004).
S50. H. J. Becker, *Contrib. Mineral. Petrol.* **65**, 45-52 (1977).
S51. G. Witt-Eickschen, H. A. Seck, K. Mezger, S. M. Eggins, R. Altherr, *J. Petrol.* **44**, 1077-1095 (2003).
S52. M. G. Best, *J. Petrol.* **16**, 212-236 (1975).
S53. D. A. Ionov, A. W. Hofmann, *Earth Planet. Sci. Lett.* **131**, 341-356 (1995).
S54. S. Y. Wass, in *The Mantle Sample: Inclusions in kimberlites and Others Volcanics* F. R. Boyd, H. O. A. Meyer, Eds. (Amer. Geophys. Union, Washington, D.C., 1979) pp. 366-373.
S55. A. Zanetti, R. Vannucci, P. Bottazzi, R. Oberti, L. Ottolini, *Chem. Geol.* **134**, 113-133 (1996).
S56. J. Fabries, J. P. Lorand, M. Guiraud, *Contrib. Mineral. Petrol.* **140**, 383-403 (2001).
S57. R. Vannucci *et al.*, *Geochim. Cosmochim. Acta* **59**, 1763-1771 (1995).
S58. G. Chazot, M. Menzies, B. Harte, *Chem. Geol.* **134**, 159-179 (1996).
S59. M. Gregoire, B. N. Moine, S. Y. O'Reilly, J. Y. Cottin, A. Giret, *J. Petrol.* **41**, 477-509 (2000).
S60. C. S. J. Shaw, J. Eyzaguirre, *Lithos* **50**, 75-95 (2000).
S61. M. Wilson, H. Downes, *J. Petrol.* **32**, 811-849 (1991).

Table S1. Experimental phase assemblages and glass compositions (in wt. %)

Run no.	T (°C)	Duration (h)	Prop.†	Phases ††	SiO_2	TiO_2	Al_2O_3	FeO*	MnO	MgO	CaO	Na_2O	K_2O	P_2O_5	H_2O	CO_2	Total
Hornblendite experiments (AG4 composition)					39.15(39)	5.39(5)	13.99(14)	10.95(22)	0.20(1)	11.89(12)	12.30(12)	2.38(7)	1.19(6)	0.42(1)	1.75(10)	0.20(10)	99.8
AG4-12	1150	64		gl;ol;cpx;sp;amph;ilm													
AG4-13	1165	64		(25)gl;(3)ol;(16)cpx;(0)sp;(57)amph;(0.3)ilm	36.80(16)	6.09(4)	12.95(4)	15.56(16)	0.33(3)	6.90(9)	10.10(9)	3.94(10)	1.30(2)	1.65(8)	2.50(26)	0.89(9)	99.01
AG4-11	1175	64		(43)gl;(4)ol;(21)cpx;(2.3)sp;(29)amph;(0.1)ilm	36.98(11)	6.63(7)	13.33(8)	14.20(13)	0.27(2)	7.57(7)	10.28(9)	3.64(5)	1.36(2)	0.97(5)	3.27(14)	1.00(4)	99.5
AG4-22r	1150/1175	25-54		(60)gl;(6)ol;(25)cpx;(3.2)sp;(6)amph;(tr)ilm	36.92(18)	6.66(8)	13.09(9)	14.54(9)	0.27(2)	7.32(10)	9.94(7)	3.81(7)	1.50(2)	1.11(6)	3.56(16)	1.17(5)	99.87
AG4-8	1190	48		(59)gl;(7)ol;(30)cpx;(3.7)sp	38.11(9)	6.93(9)	13.95(7)	12.51(9)	0.23(3)	7.60(7)	9.88(6)	3.72(10)	1.96(2)	0.69(4)	2.50(11)	0.68(3)	98.76
AG4-3	1200	24		(64)gl;(7)ol;(26)cpx;(3.2)sp	38.16(13)	6.64(6)	14.06(7)	12.16(6)	0.24(3)	8.01(4)	10.45(5)	3.48(6)	1.78(3)	0.62(5)	2.58(14)	0.74(4)	98.91
AG4-7	1225	46		(63)gl;(6)ol;(27)cpx;(3.6)sp	38.04(17)	6.84(6)	13.77(7)	12.37(11)	0.22(2)	8.02(5)	10.28(6)	3.63(6)	1.84(2)	0.66(4)	2.16(6)	0.77(2)	98.59
AG4-38	1225	48		(66)gl;(7)ol;(25)cpx;(3.3)sp	38.53(12)	6.81(9)	13.94(7)	12.59(20)	0.23(2)	8.09(6)	10.62(5)	3.43(8)	1.76(5)	0.65(3)	2.37(5)	0.71(1)	99.73
AG4-21r	1200/1225	48-48		(63)gl;(6)ol;(27)cpx;(3.6)sp	38.63(19)	6.89(8)	13.81(9)	12.37(6)	0.22(2)	8.12(5)	10.38(5)	3.49(9)	1.84(2)	0.68(5)	2.15(7)	0.78(3)	99.37
AG4-4	1250	24		(77)gl;(6)ol;(16)cpx;(1.9)sp	38.90(10)	6.24(4)	14.05(7)	11.22(12)	0.20(2)	8.98(7)	11.65(6)	3.03(11)	1.49(4)	0.54(3)	2.20(20)	0.75(20)	99.25
AG4-6	1275	25		(90)gl;(5)ol;(4)cpx;(1.1)sp	38.84(17)	5.79(7)	14.14(12)	10.53(10)	0.20(3)	9.77(13)	12.54(7)	2.71(9)	1.26(2)	0.49(3)	2.13(5)	0.74(2)	99.14
AG4-10	1285	48		(95)gl;(4)ol;(0.8)sp	39.03(15)	5.61(8)	13.98(7)	10.82(17)	0.18(2)	10.27(7)	12.66(4)	2.69(10)	1.23(2)	0.47(4)	1.97(5)	0.73(2)	99.65
AG4-20	1300	48		(97)gl;(2)ol;(0.2)sp	39.21(15)	5.53(4)	14.16(7)	10.26(11)	0.19(2)	10.93(8)	12.37(5)	2.58(8)	1.21(2)	0.46(3)	1.87(2)	1.15(1)	99.91
AG4-2	1350	24		(100)gl.	39.11(11)	5.39(6)	14.07(5)	9.76(12)	0.18(2)	11.92(8)	12.06(3)	2.57(5)	1.18(2)	0.44(1)	1.64(9)	0.95(9)	99.28
Clinopyroxene-hornblendite experiments (AG7 composition)					43.31(43)	3.59(4)	11.23(11)	7.65(15)	0.12(0)	12.53(13)	17.07(17)	1.60(5)	0.81(4)	0.05(0)	0.76(1)	0.26(1)	98.98
AG7-2	1225	48		gl;ol;cpx;sp													
AG7-1	1250	48		(37)gl;(3)ol;(58)cpx;(1.7)sp	39.51(18)	5.30(4)	13.69(9)	11.48(11)	0.17(3)	8.79(5)	11.71(10)	3.14(5)	1.88(3)	0.12(2)	2.23(7)	1.14(4)	99.16
AG7-10	1275	48		(45)gl;(3)ol;(52)cpx	40.05(15)	5.07(11)	13.40(8)	10.94(10)	0.15(3)	9.69(12)	12.98(6)	2.80(12)	1.58(6)	0.10(1)	1.71(3)	1.01(2)	99.48
AG7-4	1300	48		(54)gl;(2)ol;(44)cpx	40.81(11)	4.64(6)	13.12(9)	9.86(11)	0.15(3)	10.59(8)	14.03(4)	2.49(11)	1.27(3)	0.10(2)	1.48(3)	0.80(2)	99.33
AG7-5	1325	48		(64)gl;(1)ol;(36)cpx	41.20(13)	4.45(5)	12.81(6)	9.53(8)	0.14(2)	11.40(6)	14.54(6)	2.20(8)	1.13(4)	0.08(2)	1.25(2)	0.82(1)	99.56
AG7-8	1350	48		(79)gl;(21)cpx	42.26(11)	4.18(9)	12.20(9)	8.72(8)	0.13(2)	12.00(8)	15.58(7)	2.04(16)	0.99(3)	0.07(1)	1.06(2)	0.91(1)	100.13
AG7-11	1375	48		(93)gl;(7)cpx	42.98(12)	3.91(7)	11.64(6)	7.87(10)	0.12(1)	12.35(11)	16.46(6)	1.84(13)	0.89(2)	0.06(1)	0.77(2)	0.60(1)	99.49
AG7-12	1400	48		(100)gl	44.10(14)	3.63(6)	11.37(5)	6.89(13)	0.13(2)	12.63(8)	17.01(8)	1.70(7)	0.80(2)	0.06(2)	0.76(1)	1.01(1)	100.1
Hornblendite - DMM1 sandwich experiments (DMM1 composition)					44.91	0.04	2.38	8.34	0.13	41.59	2.14	0.06	0.01				99.6
AG4-16L	1225	48	0.391	(31)gl;(51)ol;(17)cpx;(1.2)sp	43.05(13)	5.71(8)	15.57(12)	8.09(8)	0.15(1)	9.54(38)	9.34(9)	2.77(8)	1.45(2)	0.53(3)	2.35(4)	0.73(1)	99.28
AG4-26L	1250	48	0.321	(30)gl;(54)ol;(13)cpx;(0.2)sp;(4)opx	44.04(16)	4.66(8)	15.67(15)	7.74(7)	0.15(2)	10.35(12)	9.97(4)	2.32(6)	1.12(2)	0.41(3)	2.57(3)	0.46(1)	99.46
AG4-15L	1250	48	0.386	(38)gl;(51)ol;(10)cpx;(0.3)sp;(1)opx	43.21(29)	4.80(7)	15.07(13)	7.95(6)	0.16(2)	10.43(16)	10.16(6)	2.36(9)	1.11(2)	0.41(3)			95.66
AG4-24L	1275	48	0.235	(27)gl;(57)ol;(8)cpx;(tr)sp;(8)opx	44.75(17)	3.84(6)	15.58(10)	7.68(10)	0.16(3)	11.18(19)	10.66(8)	1.95(6)	0.88(2)	0.34(2)	2.00(5)	0.31(1)	99.31
AG4-14L	1275	24	0.321	(38)gl;(55)ol;(7)cpx;(tr)sp	44.59(16)	4.16(5)	14.82(15)	7.85(8)	0.16(2)	11.24(12)	10.51(7)	2.04(6)	0.93(2)	0.35(2)	1.86(8)	0.28(1)	98.79
AG4-23Lr	1200/1275	51-48	0.322	(38)gl;(56)ol;(6)cpx;(tr)sp	44.36(16)	3.87(6)	14.92(10)	7.80(10)	0.15(3)	11.42(5)	10.46(6)	1.94(7)	0.87(1)	0.31(3)		0.34(1)	96.45
AG4-17L	1300	48	0.238	(29)gl;(59)ol;(6)cpx;(tr)sp;(5)opx	44.84(19)	3.95(8)	15.02(20)	8.05(9)	0.15(3)	11.38(47)	10.92(17)	1.94(4)	0.91(2)	0.34(3)	1.42(4)	0.64(2)	99.57
AG4-9L	1300	48	0.385	(43)gl;(51)ol;(7)cpx;(tr)sp	43.95(17)	4.48(7)	14.66(11)	8.33(13)	0.17(3)	11.30(9)	10.76(11)	2.17(4)	1.00(2)	0.38(4)	1.65(8)	0.59(3)	99.45
AG4-19L	1325	48	0.252	(34)gl;(57)ol;(4)cpx;(tr)sp;(5)opx	45.22(21)	3.36(3)	13.64(17)	8.17(10)	0.18(2)	13.07(29)	10.88(11)	1.73(4)	0.74(1)	0.27(3)	1.44(2)	0.53(1)	99.22
Preliminary experiments on dehydrated hornblendite AG4																	
AG4D-33	1250	48		(46)gl;(4.8)ol;(44)cpx;(5.0)sp	38.51(18)	8.29(3)	13.02(8)	13.93(2)	0.24(7)	7.43(5)	8.84(1)	4.14(6)	2.39(7)	0.89(1)			97.68
AG4D-32	1275	48		(57)gl;(4.1)ol;(34)cpx;(4.1)sp	38.85(11)	7.42(12)	13.24(7)	13.38(12)	0.23(1)	8.25(7)	9.86(8)	3.72(8)	1.95(3)	0.66(3)			97.56
AG4D-31	1300	48		(66)gl;(3.9)ol;(27)cpx;(3.6)sp	39.15(11)	7.01(5)	13.38(8)	12.88(5)	0.23(2)	8.90(7)	10.70(8)	3.38(12)	1.67(3)	0.61(4)	0.12(1)	1.21(2)	99.22
AG4D-30	1325	48		(84)gl;(3.4)ol;(10)cpx;(2.3)sp	39.72(9)	6.16(5)	13.65(4)	11.76(9)	0.21(2)	10.10(6)	12.16(3)	2.81(11)	1.32(3)	0.49(3)	0.09(1)	1.32(2)	99.77
AG4D-28	1350	48		(96)gl;(2.3)ol;(1.4)sp	39.61(17)	5.74(8)	13.61(5)	11.11(6)	0.20(2)	10.98(7)	12.66(11)	2.59(6)	1.16(2)	0.44(4)	0.10(1)	0.89(3)	99.08

Notes. † Prop: Proportion of hornblendite AG4 relative to depleted MORB mantle (DMM1) in sandwich experiments (= AG4/(AG4+DMM1) by weight). †† Proportion of phases (in wt. %) present in experimental charge determined by least-squares mass balance (see Supporting Online Material for details of the mass balance calculation). The numbers in parentheses are standard deviations, given in terms of the least unit cited; e.g., 39.15(39) = 39.15±0.39. Abbreviations: gl = glass; ol = olivine; cpx = clinopyroxene; sp = spinel; opx = orthopyroxene; amph = amphibole; ilm = ilmenite.

Table S2. Compositions of solid phases from the experiments

Run no.	Temperature (ºC)		n†	SiO2 (wt.%)	TiO2 (wt.%)	Al2O3 (wt.%)	FeO* (wt.%)	MnO (wt.%)	MgO (wt.%)	CaO (wt.%)	Na2O (wt.%)	K2O (wt.%)	Cr2O3 (wt.%)	Total (wt.%)
Hornblendite AG4 experiments														
AG4-12	1150	Olivine	*5*	38.17 (41)	0.21 (3)	0.19 (17)	25.05 (11)	0.43 (2)	35.38 (23)	0.48 (17)	0.06 (2)		0.02 (1)	99.98
AG4-12	1150	Amphibole	*9*	38.94 (34)	5.05 (8)	15.61 (10)	9.19 (13)	0.13 (2)	13.24 (10)	11.58 (7)	2.53 (6)	1.50 (4)	0.00 (0)	97.77
AG4-12	1150	Ilmenite	*10*	0.04 (1)	52.56 (21)	0.90 (2)	36.34 (13)	0.51 (2)	8.46 (11)	0.48 (7)	0.01 (1)		0.00 (0)	99.29
AG4-13	1165	Olivine	*1*	38.44 (0)	0.36 (0)	0.73 (0)	23.24 (0)	0.39 (0)	35.94 (0)	1.32 (0)	0.10 (0)		0.01 (0)	100.54
AG4-13	1165	Clinopyroxene	*7*	45.60 (32)	3.57 (17)	10.32 (30)	6.54 (23)	0.17 (2)	11.95 (11)	20.58 (30)	1.15 (5)		0.03 (0)	99.91
AG4-13	1165	Amphibole	*7*	38.70 (33)	5.59 (16)	15.37 (24)	9.14 (12)	0.13 (2)	12.93 (8)	11.48 (7)	2.54 (5)	1.62 (7)	0.01 (1)	97.5
AG4-13	1165	Ilmenite	*8*	0.20 (16)	52.21 (56)	1.00 (10)	35.89 (21)	0.48 (3)	8.61 (10)	0.66 (22)	0.05 (4)		0.01 (0)	99.1
AG4-11	1175	Olivine	*8*	39.20 (20)	0.14 (2)	0.07 (2)	20.96 (10)	0.34 (2)	39.29 (11)	0.33 (3)	0.02 (1)		0.02 (1)	100.36
AG4-11	1175	Clinopyroxene	*7*	46.40 (21)	3.56 (12)	10.39 (19)	5.38 (5)	0.15 (2)	12.36 (10)	21.28 (10)	0.97 (2)		0.04 (1)	100.54
AG4-11	1175	Spinel	*9*	0.07 (1)	1.15 (2)	63.49 (17)	17.41 (13)	0.15 (1)	18.96 (8)	0.15 (2)	0.01 (1)		0.05 (1)	101.43
AG4-11	1175	Amphibole	*10*	39.47 (13)	5.69 (9)	15.64 (10)	7.70 (10)	0.10 (2)	13.81 (7)	11.66 (6)	2.29 (5)	1.89 (5)	0.01 (1)	98.25
AG4-11	1175	Ilmenite	*6*	0.10 (6)	53.42 (43)	1.04 (4)	33.40 (33)	0.43 (3)	10.19 (11)	0.58 (8)	0.03 (0)		0.01 (1)	99.2
AG4-22r	1175	Olivine	*6*	38.88 (11)	0.11 (2)	0.06 (1)	21.91 (21)	0.35 (2)	38.74 (24)	0.34 (2)	0.02 (2)		0.02 (1)	100.43
AG4-22r	1175	Clinopyroxene	*7*	46.33 (49)	3.53 (25)	10.53 (48)	5.79 (21)	0.16 (1)	12.18 (15)	21.08 (4)	1.06 (4)		0.04 (1)	100.7
AG4-22r	1175	Spinel	*10*	0.08 (2)	1.15 (5)	63.32 (32)	17.91 (8)	0.16 (2)	18.59 (14)	0.14 (4)	0.01 (1)		0.05 (1)	101.42
AG4-22r	1175	Amphibole	*14*	39.09 (42)	5.05 (39)	15.40 (22)	8.93 (46)	0.13 (2)	13.18 (13)	11.62 (10)	2.45 (10)	1.58 (17)	0.01 (1)	97.44
AG4-22r	1175	Ilmenite	*6*	0.10 (4)	53.35 (27)	1.01 (2)	33.77 (17)	0.43 (2)	10.21 (6)	0.56 (12)	0.02 (1)		0.01 (1)	99.45
AG4-8	1190	Olivine	*4*	39.62 (4)	0.17 (2)	0.08 (3)	19.08 (18)	0.29 (2)	41.64 (44)	0.36 (6)	0.03 (2)		0.03 (1)	101.29
AG4-8	1190	Clinopyroxene	*14*	45.78 (95)	4.12 (41)	11.06 (61)	5.58 (48)	0.13 (2)	12.46 (48)	21.21 (25)	1.05 (6)		0.04 (1)	101.42
AG4-8	1190	Spinel	*5*	0.19 (13)	1.20 (2)	63.23 (33)	15.49 (11)	0.13 (1)	19.91 (7)	0.22 (6)	0.03 (1)		0.04 (1)	100.44
AG4-3	1200	Olivine	*13*	39.65 (36)	0.19 (2)	0.14 (8)	17.65 (13)	0.26 (3)	42.09 (19)	0.40 (4)	0.02 (1)		0.02 (1)	100.44
AG4-3	1200	Clinopyroxene	*13*	45.45 (65)	3.87 (25)	11.10 (38)	5.41 (70)	0.12 (2)	12.39 (32)	21.24 (41)	0.95 (9)		0.03 (1)	100.56
AG4-3	1200	Spinel	*8*	0.24 (11)	1.18 (5)	63.81 (37)	14.67 (7)	0.13 (1)	20.41 (13)	0.25 (10)	0.02 (2)		0.05 (1)	100.75
AG4-7	1225	Olivine	*5*	39.49 (26)	0.19 (4)	0.34 (32)	18.23 (15)	0.27 (3)	42.69 (23)	0.44 (8)	0.03 (2)		0.02 (0)	101.71
AG4-7	1225	Clinopyroxene	*8*	46.03 (42)	3.89 (24)	10.83 (45)	4.86 (6)	0.13 (2)	12.86 (21)	21.49 (9)	1.01 (3)		0.04 (1)	101.13
AG4-7	1225	Spinel	*6*	0.17 (6)	1.09 (6)	63.56 (28)	14.69 (12)	0.12 (2)	20.33 (13)	0.20 (5)	0.03 (2)		0.05 (1)	100.24
AG4-38	1225	Olivine	*4*	39.61 (24)	0.11 (3)	0.16 (13)	17.59 (15)	0.26 (3)	42.83 (16)	0.44 (11)	0.03 (2)		0.00 (1)	101.02
AG4-38	1225	Clinopyroxene	*15*	46.12 (35)	3.47 (20)	10.95 (29)	4.59 (25)	0.11 (2)	12.64 (16)	21.44 (29)	0.94 (5)		0.01 (1)	100.28
AG4-38	1225	Spinel	*8*	0.19 (6)	1.02 (2)	64.43 (9)	13.65 (21)	0.11 (1)	20.55 (10)	0.14 (4)	0.01 (1)		0.05 (1)	100.15
AG4-21r	1225	Olivine	*4*	39.58 (5)	0.16 (3)	0.10 (4)	17.73 (9)	0.27 (2)	42.54 (3)	0.36 (3)	0.02 (1)		0.01 (0)	100.76
AG4-21r	1225	Clinopyroxene	*13*	45.98 (35)	4.04 (22)	10.89 (34)	5.08 (28)	0.13 (2)	12.39 (23)	20.92 (33)	1.08 (5)		0.04 (1)	100.54
AG4-21r	1225	Spinel	*16*	0.13 (8)	1.07 (3)	64.84 (26)	14.50 (10)	0.13 (1)	20.20 (16)	0.21 (5)	0.05 (4)		0.05 (2)	101.17
AG4-4	1250	Olivine	*8*	39.81 (16)	0.20 (8)	0.17 (13)	15.40 (9)	0.24 (2)	43.76 (32)	0.48 (10)	0.03 (2)		0.02 (1)	100.1
AG4-4	1250	Clinopyroxene	*7*	44.86 (115)	3.55 (52)	12.30 (124)	4.78 (53)	0.10 (2)	12.86 (25)	21.18 (60)	0.79 (6)		0.04 (0)	100.45
AG4-4	1250	Spinel	*10*	0.14 (7)	0.86 (4)	63.85 (26)	11.89 (12)	0.11 (1)	21.07 (14)	0.23 (7)	0.01 (1)		0.05 (1)	98.21
AG4-6	1275	Olivine	*7*	40.14 (42)	0.10 (4)	0.10 (3)	13.90 (16)	0.21 (2)	45.95 (12)	0.41 (4)	0.03 (2)		0.02 (1)	100.84
AG4-6	1275	Clinopyroxene	*2*	47.00 (149)	2.81 (51)	10.30 (157)	3.83 (18)	0.11 (1)	13.92 (83)	22.23 (12)	0.68 (1)		0.05 (1)	100.93
AG4-6	1275	Spinel	*10*	0.09 (2)	0.68 (2)	65.70 (27)	11.14 (13)	0.10 (1)	22.64 (15)	0.04 (3)	0.00 (0)		0.14 (1)	100.54
AG4-10	1285	Olivine	*6*	40.92 (23)	0.09 (2)	0.10 (1)	13.62 (11)	0.20 (3)	45.89 (16)	0.41 (3)	0.01 (1)		0.03 (1)	101.28
AG4-10	1285	Spinel	*9*	0.13 (4)	0.70 (2)	65.84 (27)	10.96 (16)	0.11 (1)	22.64 (13)	0.09 (5)	0.01 (1)		0.17 (1)	100.63
AG4-20	1300	Olivine	*6*	40.82 (25)	0.09 (3)	0.11 (1)	12.22 (22)	0.21 (2)	46.46 (8)	0.39 (3)	0.03 (1)		0.02 (0)	100.34
AG4-20	1300	Spinel	*11*	0.10 (1)	0.67 (2)	66.96 (26)	10.13 (13)	0.09 (1)	23.13 (9)	0.04 (2)	0.00 (1)		0.19 (1)	101.32
Cpx-hornblendite AG7 experiments														
AG7-2	1225	Olivine	*5*	39.45 (24)	0.10 (5)	0.09 (5)	16.86 (10)	0.19 (1)	44.44 (25)	0.47 (5)	0.02 (2)		0.00 (1)	101.64
AG7-2	1225	Clinopyroxene	*23*	47.41 (93)	2.53 (35)	9.22 (119)	5.03 (79)	0.09 (3)	13.04 (99)	22.39 (90)	0.79 (12)		0.05 (2)	100.56
AG7-2	1225	Spinel	*7*	0.18 (4)	0.77 (2)	64.77 (24)	12.02 (15)	0.08 (1)	21.31 (7)	0.18 (2)	0.01 (1)		0.38 (3)	99.73
AG7-1	1250	Olivine	*13*	39.98 (25)	0.07 (2)	0.10 (5)	15.76 (16)	0.18 (1)	44.97 (18)	0.54 (6)	0.02 (1)		0.01 (1)	101.65
AG7-1	1250	Clinopyroxene	*21*	47.90 (87)	2.37 (33)	9.00 (117)	4.74 (81)	0.09 (3)	13.20 (76)	22.77 (67)	0.71 (7)		0.05 (2)	100.85
AG7-1	1250	Spinel	*2*	0.17 (2)	0.79 (1)	65.69 (1)	12.78 (6)	0.08 (0)	20.63 (4)	0.18 (0)	0.02 (1)		0.40 (5)	100.74
AG7-10	1275	Olivine	*15*	40.30 (24)	0.09 (2)	0.10 (1)	13.93 (10)	0.16 (1)	45.89 (25)	0.53 (6)	0.03 (1)		0.01 (1)	101.04
AG7-10	1275	Clinopyroxene	*20*	47.36 (114)	2.45 (58)	9.43 (141)	4.02 (74)	0.08 (2)	13.77 (72)	22.12 (58)	0.66 (6)		0.05 (2)	99.95
AG7-4	1300	Olivine	*10*	40.56 (22)	0.09 (2)	0.10 (2)	12.24 (11)	0.15 (1)	48.60 (25)	0.56 (6)	0.02 (1)		0.01 (1)	102.32
AG7-4	1300	Clinopyroxene	*25*	48.46 (93)	2.04 (33)	8.55 (79)	3.77 (98)	0.07 (2)	14.77 (102)	22.34 (29)	0.55 (5)		0.06 (2)	100.64
AG7-5	1325	Olivine	*7*	40.75 (9)	0.08 (1)	0.10 (1)	11.13 (5)	0.13 (1)	49.30 (12)	0.58 (4)	0.02 (1)		0.01 (1)	102.11
AG7-5	1325	Clinopyroxene	*26*	49.23 (94)	1.81 (35)	7.88 (66)	3.41 (94)	0.07 (2)	15.24 (109)	22.44 (29)	0.49 (4)		0.06 (2)	100.66
AG7-8	1350	Clinopyroxene	*10*	50.04 (53)	1.58 (20)	7.37 (54)	2.58 (4)	0.05 (2)	15.74 (19)	22.45 (12)	0.42 (1)		0.10 (1)	100.34
AG7-11	1375	Clinopyroxene	*10*	50.46 (18)	1.30 (7)	6.28 (26)	2.32 (3)	0.05 (1)	16.18 (12)	22.64 (5)	0.38 (1)		0.13 (1)	99.75
Hornblendite AG4 - Depleted MORB mantle DMM1 sandwich experiments														
AG4-16L	1225	Olivine	*13*	40.84 (17)	0.08 (2)	0.11 (9)	11.81 (7)	0.16 (2)	46.76 (24)	0.23 (3)	0.01 (1)		0.06 (2)	100.24
AG4-16L	1225	Clinopyroxene	*11*	49.57 (175)	1.71 (76)	8.74 (149)	4.20 (19)	0.12 (2)	16.07 (121)	19.05 (99)	0.82 (6)		0.57 (26)	100.86
AG4-16L	1225	Spinel	*3*	0.55 (35)	0.74 (3)	64.23 (90)	9.72 (4)	0.06 (1)	22.93 (20)	0.08 (4)	0.01 (1)		2.32 (48)	100.79
AG4-16L	1225	Orthopyroxene	*7*	54.20 (75)	0.33 (15)	6.17 (77)	7.05 (27)	0.15 (2)	31.31 (65)	1.45 (32)	0.11 (1)		0.46 (5)	101.25
AG4-15L	1250	Olivine	*19*	40.90 (49)	0.07 (2)	0.09 (5)	11.12 (15)	0.16 (2)	47.28 (83)	0.28 (15)	0.02 (1)		0.07 (1)	100.1
AG4-15L	1250	Clinopyroxene	*17*	50.00 (72)	1.41 (36)	7.81 (71)	4.05 (14)	0.13 (2)	16.57 (66)	19.30 (56)	0.66 (4)		0.77 (14)	100.7
AG4-15L	1250	Spinel	*11*	0.09 (1)	0.77 (4)	57.39 (206)	10.31 (24)	0.11 (1)	22.05 (29)	0.07 (5)	0.00 (0)		9.70 (196)	100.6
AG4-26L	1250	Olivine	*26*	40.80 (37)	0.06 (2)	0.08 (2)	11.24 (8)	0.16 (1)	48.32 (23)	0.23 (2)	0.01 (0)		0.03 (1)	100.94
AG4-26L	1250	Clinopyroxene	*12*	49.93 (67)	1.48 (22)	8.45 (36)	4.05 (7)	0.12 (1)	17.14 (28)	18.06 (35)	0.67 (3)		0.44 (8)	100.33
AG4-26L	1250	Spinel	*4*	0.47 (42)	0.66 (8)	59.31 (137)	9.60 (31)	0.11 (2)	22.61 (25)	0.14 (7)	0.03 (5)		7.64 (134)	100.69
AG4-26L	1250	Orthopyroxene	*9*	54.70 (58)	0.27 (10)	5.63 (76)	6.62 (15)	0.14 (1)	31.80 (50)	1.46 (33)	0.09 (1)		0.33 (5)	101.04
AG4-14L	1275	Olivine	*18*	40.52 (52)	0.06 (2)	0.07 (2)	10.38 (9)	0.16 (2)	48.29 (23)	0.24 (2)	0.02 (1)		0.11 (1)	100
AG4-14L	1275	Clinopyroxene	*15*	50.86 (49)	0.90 (20)	6.62 (35)	4.18 (10)	0.13 (1)	18.25 (38)	17.85 (34)	0.57 (3)		1.11 (5)	100.49
AG4-14L	1275	Spinel	*11*	0.16 (8)	0.83 (5)	50.53 (278)	10.44 (30)	0.13 (1)	21.63 (47)	0.08 (4)	0.01 (1)		16.70 (281)	100.62
AG4-23Lr	1275	Olivine	*30*	41.72 (16)	0.05 (1)	0.07 (2)	10.27 (8)	0.16 (2)	47.81 (20)	0.25 (5)	0.01 (1)		0.11 (1)	100.49
AG4-23Lr	1275	Clinopyroxene	*12*	51.29 (95)	1.15 (57)	7.59 (105)	4.00 (59)	0.13 (3)	17.39 (129)	18.24 (101)	0.56 (6)		0.85 (15)	101.24
AG4-23Lr	1275	Spinel	*8*	0.26 (3)	0.71 (4)	53.00 (198)	9.37 (34)	0.13 (2)	22.05 (36)	0.05 (3)	0.00 (1)		14.42 (211)	100.02
AG4-24L	1275	Olivine	*21*	40.39 (16)	0.06 (2)	0.08 (2)	10.48 (5)	0.15 (1)	48.77 (16)	0.25 (3)	0.01 (1)		0.05 (1)	100.25
AG4-24L	1275	Clinopyroxene	*13*	49.53 (130)	1.01 (34)	7.71 (80)	4.09 (25)	0.12 (1)	17.88 (64)	17.45 (58)	0.54 (7)		0.60 (8)	98.96
AG4-24L	1275	Spinel	*7*	0.12 (3)	0.64 (3)	54.99 (51)	9.47 (4)	0.12 (1)	22.09 (10)	0.09 (4)	0.00 (1)		13.13 (58)	100.74
AG4-24L	1275	Orthopyroxene	*4*	53.92 (88)	0.18 (4)	5.26 (25)	6.29 (21)	0.13 (1)	32.35 (9)	1.30 (39)	0.08 (2)		0.37 (2)	99.88
AG4-9L	1300	Olivine	*23*	41.39 (21)	0.06 (2)	0.08 (2)	10.86 (12)	0.17 (2)	48.54 (17)	0.27 (3)	0.02 (1)		0.10 (1)	101.57
AG4-9L	1300	Clinopyroxene	*13*	50.99 (50)	1.05 (18)	7.52 (32)	4.13 (8)	0.13 (2)	17.72 (56)	18.03 (68)	0.64 (3)		0.93 (4)	101.13
AG4-9L	1300	Spinel	*7*	0.10 (1)	0.80 (4)	54.49 (112)	10.23 (14)	0.11 (2)	21.72 (19)	0.09 (3)	0.00 (1)		12.91 (112)	100.51
AG4-17L	1300	Olivine	*16*	41.24 (31)	0.06 (1)	0.10 (6)	10.10 (8)	0.15 (2)	48.46 (27)	0.27 (2)	0.02 (2)		0.11 (1)	100.57
AG4-17L	1300	Clinopyroxene	*10*	50.44 (48)	1.01 (13)	7.54 (20)	4.14 (11)	0.14 (2)	18.55 (20)	16.93 (30)	0.59 (2)		1.07 (19)	100.46
AG4-17L	1300	Spinel	*9*	0.13 (2)	0.72 (3)	52.48 (95)	9.99 (18)	0.13 (2)	21.50 (30)	0.10 (3)	0.00 (0)		15.76 (111)	100.86
AG4-17L	1300	Orthopyroxene	*7*	54.38 (50)	0.25 (8)	5.67 (65)	6.54 (8)	0.14 (1)	31.77 (53)	1.71 (34)	0.08 (2)		0.61 (6)	101.16
AG4-19L	1325	Olivine	*19*	41.02 (26)	0.05 (1)	0.09 (1)	9.66 (7)	0.14 (2)	48.96 (11)	0.26 (1)	0.02 (1)		0.17 (1)	100.41
AG4-19L	1325	Clinopyroxene	*5*	44.61 (96)	4.08 (68)	13.16 (128)	6.94 (77)	0.18 (2)	13.58 (217)	15.87 (121)	0.75 (14)		0.45 (14)	99.64
AG4-19L	1325	Spinel	*14*	0.13 (4)	0.85 (3)	42.24 (85)	10.63 (11)	0.16 (2)	20.74 (24)	0.08 (4)	0.00 (0)		25.74 (94)	100.59
AG4-19L	1325	Orthopyroxene	*4*	54.33 (30)	0.39 (12)	5.31 (21)	5.92 (4)	0.15 (2)	31.03 (28)	2.28 (16)	0.10 (0)		1.18 (4)	100.73

Notes. † n: number of individual analyses used to calculate the average composition and the standard deviation. The numbers in parentheses are standard deviations, given in terms of the least unit cited.

Table S3. Trace-element compositions of the experimental glasses

Run no.	T (°C)	F†	Rb (ppm)	Ba (ppm)	Th (ppm)	U (ppm)	Nb (ppm)	La (ppm)	Ce (ppm)	Pb (ppm)	Pr (ppm)	Sr (ppm)	Nd (ppm)	Sm (ppm)	Zr (ppm)	Hf (ppm)	Eu (ppm)	Gd (ppm)	Tb (ppm)	Dy (ppm)	Y (ppm)	Ho (ppm)	Er (ppm)	Tm (ppm)	Yb (ppm)	Lu (ppm)
Hornblendite AG4 experiments																										
AG4-13	1165	25	16.7	567	14.6	3.1	372	160.5	348.9	14.3	36.4	1366	130.8	21.1	536	9.6	6.3	16.9	2.08	11.0	51.9	2.07	5.07	0.77	3.82	0.47
AG4-11	1175	43	11.4	538	8.9	1.8	249	103.2	243.8	7.1	27.3	1217	102.5	18.1	370	8.2	5.3	14.3	1.67	9.3	41.8	1.62	4.10	0.55	3.61	0.49
AG4-22r	1150/1175	36	12.4	609	10.9	2.2	297	120.8	279.2	10.7	30.6	1344	111.6	18.9	411	8.6	5.9	15.1	1.87	10.1	44.5	1.66	4.36	0.57	3.87	0.54
AG4-8	1190	59	12.0	640	6.9	1.5	213	83.9	200.6	6.3	22.8	1320	86.3	15.2	308	7.3	4.9	12.8	1.55	8.6	38.2	1.52	3.64	0.51	3.37	0.47
AG4-3	1200	64	11.0	567	5.8	1.2	186	71.1	177.4	5.7	20.3	1192	79.8	14.3	266	6.2	4.4	11.1	1.40	7.9	34.5	1.32	3.45	0.43	2.73	0.39
AG4-7	1225	63	11.2	623	6.6	1.4	205	81.3	198.3	5.5	22.5	1282	85.8	15.8	293	7.0	5.0	11.9	1.50	8.4	36.8	1.45	3.72	0.47	3.15	0.44
AG4-38	1225	66	10.1	556	6.7	1.3	185	80.6	182.1	5.8	21.7	1224	87.7	15.2	313	7.8	4.9	13.1	1.64	9.3	40.8	1.60	3.91	0.51	3.26	0.44
AG4-21r	1200/1225	63	11.0	609	7.1	1.4	206	82.3	193.5	5.1	22.5	1280	88.2	17.0	319	7.7	5.0	13.0	1.71	9.1	40.9	1.56	4.07	0.50	3.40	0.45
AG4-4	1250	77	8.3	458	5.2	1.0	151	62.1	150.6	4.3	17.6	1002	71.5	13.4	245	6.2	4.2	11.1	1.35	7.8	34.0	1.34	3.34	0.42	2.78	0.38
AG4-6	1275	90	7.4	407	4.7	0.9	136	55.9	137.6	4.0	16.4	911	65.9	12.6	226	5.8	4.0	10.6	1.29	7.4	33.1	1.26	3.17	0.40	2.64	0.35
AG4-10	1285	95	7.1	390	4.6	0.9	130	55.5	133.5	3.3	16.2	899	66.1	12.9	234	6.0	4.0	10.9	1.36	7.6	33.8	1.34	3.27	0.41	2.81	0.37
AG4-20	1300	97	6.8	376	5.0	0.9	133	57.9	130.2	2.9	15.9	877	68.0	13.3	253	6.7	4.0	11.7	1.48	8.4	37.1	1.45	3.59	0.48	2.86	0.39
AG4-2	1350	100	7.0	384	4.3	0.9	128	52.7	130.7	3.3	15.5	863	63.3	12.2	211	5.6	3.8	9.7	1.26	7.0	30.2	1.21	3.07	0.40	2.54	0.33
Clinopyroxene-hornblendite AG4 experiments																										
AG7-1	1250	37	19.1	618	0.9	0.3	41	21.6	58.4	4.1	8.0	939	37.4	7.9	152	4.4	2.7	7.0	0.91	5.0	21.8	0.89	2.05	0.26	1.51	0.20
AG7-10	1275	45	15.2	522	0.8	0.2	33	20.4	52.8	3.5	7.7	831	36.5	7.8	147	4.6	2.7	7.0	0.93	5.4	22.9	0.92	2.26	0.28	1.65	0.23
AG7-4	1300	54	11.8	422	0.6	0.2	27	16.8	44.7	2.8	6.5	693	31.0	7.3	128	4.2	2.4	6.5	0.87	5.0	21.3	0.85	2.03	0.25	1.41	0.20
AG7-5	1325	64	10.5	380	0.6	0.2	25	15.5	41.9	2.4	6.2	633	29.8	7.1	122	4.0	2.3	6.3	0.85	4.9	20.7	0.82	2.02	0.24	1.46	0.18
AG7-8	1350	79	9.5	332	0.5	0.2	22	13.7	37.7	2.2	5.7	574	27.3	6.6	107	3.7	2.2	5.8	0.79	4.4	18.2	0.74	1.85	0.23	1.25	0.17
AG7-11	1375	93	8.7	300	0.4	0.1	20	12.3	35.3	1.9	5.3	519	24.6	6.1	84	2.9	2.0	4.9	0.66	3.6	14.7	0.59	1.46	0.18	0.99	0.14
AG7-12	1400	100	8.1	275	0.4	0.1	18	11.2	32.1	1.7	4.8	500	24.2	5.8	96	3.5	2.1	5.7	0.71	4.2	18.0	0.73	1.79	0.21	1.27	0.16
Hornblendite AG4 - Depleted MORB mantle DMM1 sandwich experiments																										
AG4-16L	1225	31	8.8	456	5.8	1.1	159	65.1	150.5	5.4	17.8	993	70.4	13.7	299	7.6	3.9	11.0	1.41	7.4	36.2	1.36	3.32	0.51	2.96	0.41
AG4-26L	1250	30	6.5	362	3.8	0.8	121	47.8	120.0	4.0	13.8	782	54.4	10.2	186	4.6	3.2	7.4	0.96	5.4	25.6	0.96	2.37	0.29	2.08	0.27
AG4-15L	1250	38	6.2	348	4.4	0.8	117	49.3	115.1	3.8	13.8	768	55.0	10.6	222	5.8	3.2	8.9	1.14	6.2	29.9	1.15	2.85	0.37	2.43	0.30
AG4-24L	1275	27	4.8	281	3.2	0.6	94	39.0	93.4	3.2	11.2	625	46.6	8.6	161	4.1	2.7	6.4	0.91	5.3	23.9	0.85	2.05	0.27	1.91	0.25
AG4-14L	1275	38	5.7	298	3.9	0.7	101	43.8	98.9	3.3	12.1	673	50.2	10.0	213	5.8	2.9	9.2	1.13	6.2	30.0	1.11	2.79	0.39	2.34	0.31
AG4-23Lr	1250/1275	38	5.5	284	3.4	0.7	99	40.4	96.5	3.1	11.4	630	46.0	9.1	168	4.3	2.8	7.3	0.98	5.4	25.0	0.96	2.32	0.31	2.03	0.27
AG4-17L	1300	29	5.9	302	3.9	0.7	108	43.9	101.3	4.1	12.0	676	47.7	10.2	215	5.8	2.8	7.9	1.04	5.7	28.2	0.91	2.65	0.36	2.62	0.26
AG4-9L	1300	43	5.9	333	3.6	0.8	109	44.9	112.1	3.6	13.0	723	51.0	9.6	184	4.7	3.1	7.7	1.01	5.6	25.2	0.96	2.34	0.31	2.10	0.27
AG4-19L	1325	34	4.7	236	3.1	0.6	84	35.6	81.0	3.0	9.9	540	40.5	7.8	168	4.3	2.6	6.7	0.91	5.0	24.1	0.87	2.27	0.31	1.86	0.29
BCR2g (USGS standard)‡																										
Mean value	(*n*=20)		52.6	673	5.5	1.8	12.2	23.9	53.7	11.3	6.5	328	27.0	6.14	158	4.3	1.82	6.0	0.90	5.9	30.7	1.15	3.26	0.45	3.22	0.46
Standard deviation (1σ)			2.3	15	0.4	0.1	0.4	1.0	1.5	0.7	0.2	4	0.9	0.49	14	0.4	0.07	0.6	0.08	0.6	3.0	0.14	0.38	0.06	0.31	0.07

Notes. † Glass proportion (in wt. %) in each experiments (from mass balance). ‡ Average composition of BCR2g measured during all analytical sessions and treated as an unknown during data reduction.